Current Development in Oceanography
Special Issue of PEACE Symposium
Published Online: October 2011
Volume 2, Number 2, 2011, Pages 85-103
Available online at http://pphmj.com/journals/cdo.htm

STATISTICAL PATTERNS OF SATELLITE WIND STRESS AND CURL OVER THE JAPAN/EAST SEA

O. O. TRUSENKOVA

V.I. Il'ichev Pacific Oceanological Institute
43 Baltiyskaya Str., Vladivostok, 690041, Russia
e-mail: trolia@poi.dvo.ru

Abstract

Contemporary regime of the East Asia monsoon around the Japan/East Sea is studied, using data from the 0.5°-gridded 6-hour global QSCAT/NCEP Blended Ocean Winds data set spanning the period from July 1999 through July 2009. Wind stress vectors are decomposed to empirical orthogonal functions (EOF) in the complex form, based on spatial correlations. Both original and low-pass filtered, with the 7-day cut-off period, stresses yield the same leading EOF modes, beyond the synoptic time scale. EOF 1 accounts for the general monsoon conditions, with characteristic wind directions, seasonal shifts, and stress and curl spatial patterns. Contributions from the higher modes are not significant. Typical wind stress patterns are derived using statistics of wind directions, beyond the synoptic time scale. They are verified by the independent scalar EOF analysis of wind stress curl based on the same QSCAT/NCEP data set. Winter pattern is the leading curl mode, with fine features resolved, related to coastal orographic gaps. The second and third modes together

Keywords and phrases: East Asia monsoon, empirical orthogonal functions, histogram, Japan/East Sea, QSCAT scatterometry, wavelet transform, wind stress and curl.

Communicated by Hyo Choi

Received April 21, 2011

represent summer monsoon and monsoon change periods. These curl patterns are consistent with those computed from typical (average) wind stresses.

1. Introduction

Remote sensing has proved to be a powerful source of information on the Earth surface and atmosphere. In particular, satellite scatterometry measurements make it possible to derive both speed and direction of wind near the water surface. From July 1999 through October 2009 observations made by the Seawinds instrument onboard the QuickSCAT satellite has provided data on surface ocean winds twice a day with the resolution of 1/4° and 1/8° within satellite swaths. However, there are no data in areas of the swath divergence. Spot gaps also occur due to rain effects on wind retrieval. For some applications, such as numerical modeling of the ocean, data gaps are undesirable. To fill in gaps, satellite data can be merged with reanalysis outputs. An example of such a global product is the QSCAT/NCEP Blended Ocean Winds from Colorado Research Associates, providing fields over ocean and land.

The Japan/East Sea (JES) is located in the region of the East Asia monsoon and the atmospheric conditions there are rather stable in winter, with the prevailing northwestern (NW) winds interrupted by cyclones. In contrast, winds are highly variable during the summer monsoon, with frequently passing weather systems and strong intra-seasonal variability beyond the synoptic time scale [3-5], resulting in underestimated values in monthly fields [3, 8]. Regular high-resolution satellite data, available for the decade by now, make possible detection of statistical wind patterns.

The Empirical Orthogonal Function (EOF) analysis of wind stress over the JES and adjacent land was previously applied to the 1°-gridded 6-hour NCEP/NCAR product for 1998–2005, the SeaWiFS Project Ancillary Data, freely available on the Internet. It was shown that the leading EOF mode of wind variability over the JES accounted for the general wind directions, representing the conditions of the East Asia monsoon, and typical patterns

differing in wind directions and curl distributions were derived. The results were consistent with empirical (expert) typification [6]. As expected, wind was weaker in summer than in winter but still several times stronger than it could be inferred from monthly mean stresses [3, 8], consistent with ship observations [5]. It was also shown that the summer wind had a considerable impact upon the circulation in the JES [10]. However, the leading mode covered less than 30% of the total variance, probably due to high variance fraction related to weather systems, but it was possible that the higher modes affected the results. Typical patterns also needed more justification, while difficulties in quantitative verification mostly resulted from coarse spatial resolution.

The purpose of this study is to verify the previous results using merged satellite and reanalysis product of original and low-pass filtered, with synoptic variability removed, wind stresses. Stress vectors are decomposed to EOF, in the complex form, and statistics of leading modes, beyond the synoptic time scale, provide a ground for aggregation of 6-hour fields into typical patterns. The increased spatial resolution of satellite data makes possible an independent EOF analysis of wind stress curl for verification of curl distributions derived from stress spatial patterns.

2. Data and Methods

2.1. Wind data

The 0.5°-gridded 6-hour QSCAT/NCEP Blended Ocean Winds product is available on the Internet (http://dss.ucar.edu/datasets/ds744.4/). The data on zonal and meridional 10-m wind components span the period from July 1999 though July 2009, most of the QSCAT satellite life time. Data on February 29 in 2000, 2004, and 2008 were excluded for the sake of application in oceanic models. The area of 34°-53°N, 127°-143°E, with 1287 boxes, includes the JES and adjacent land. When the data set was generated, the satellite data were used where and when they were available, otherwise the optimal interpolation was applied, providing data over ocean and land (see details on data processing on the Web site). Wind stresses were

computed using the bulk formula. Curl values were computed at box centers by central differencing from the stresses at the corners over the sea surface only, totaling to 386 curl boxes, with the same resolution of 0.5°.

2.2. Filtering

Low-pass filtering was performed using wavelet transform, with the Morlet mother wavelet of the 6th order. Wind stress time series in every grid box were reconstructed by the inverse wavelet transform, eliminating effects of weather systems by using periods (scales) beyond 7 days. For comparison, stresses filtered with the cut-off period of 15 days were decomposed to EOF, yielding the same leading modes but with larger fraction of the total variance accounted for by EOF 1. Periods beyond 40 days were retained in wind stress curls to enable non-degenerate eigenspectrum. Decomposition of curls filtered with the 30-day cut-off period yielded the same results, although with lower eigenvalues.

2.3. EOF analysis

Wind stress vectors were decomposed to complex EOF, using zonal and meridional components as real and imagery parts, respectively [9]:

$$X(\mathbf{r}, t) = \sum (A_k(\mathbf{r}))^* B_k(t),$$

where $X(\mathbf{r}, t) = U(\mathbf{r}, t) + iV(\mathbf{r}, t)$ represents wind stress vectors, U and V are zonal and meridional components, respectively. $A_k(\mathbf{r}) = A_k(\mathbf{r})e^{-i\varphi k(\mathbf{r})}$ and $B_k(t) = B_k(t)e^{-i\phi k(t)}$ are eigenvectors (EOF) and principal components (PC), respectively, A_k / B_k are spatial/temporal amplitudes and φ_k / ϕ_k are spatial/temporal phases. The asterisk denotes the complex conjugate, $k = 1, 2, ..., M$ is the mode number, $\mathbf{r}$ represents the spatial coordinates (longitudes and latitudes), M is the number of boxes, t is time, and i is imaginary unity. Phase, increasing counterclockwise from –180° to 180°, determines stress shear in space and time, both limits referred to the same angle.

Eigenvalues and eigenvectors are derived from spatial correlations rather than from more common covariances [9]. However, correlation-like similarity measures are widely used in other multivariate techniques of data analysis. The root-mean-square pre-normalization provided by correlations enables identification of low amplitude signals, in particular weak winds. Wind stress curls are decomposed to the scalar (conventional) EOF, based on correlations.

Three leading EOF modes derived from the original wind stress vectors, two modes from the low-pass stresses, and two modes from wind stress curls pass the Monte Carlo test, i.e., the corresponding eigenvalues are non-random [9]. They are also non-degenerate in the sense of errors ([9]; Table 1; Figures 1(a), 5(a)).

3. Complex EOF Modes of Wind Stress

Three leading modes from the original wind stresses are the same as those previously derived from the 1°-gridded NCEP reanalysis [10]. However, the first and second modes only remain in the filtered data, with the same spatial and temporal patterns (Figures 1, 2). EOF 1 covers about 30% of the total variance for the original stresses and above 50% if synoptic variability is removed by low-pass filtering (Table 1). Two leading modes from stresses filtered with the 15-day cut-off period are the same, while fraction of the total variance covered by EOF 1 reaches 59% (not shown). The spatial pattern of EOF 1 is rather uniform, with a broad amplitude maximum and nearly constant phase (Figure 1(b)). Temporal amplitude reveals regular annual cycles, with the strong (weak) wind in winter (summer) but also strong interannual and intraseasonal variability, while synoptic variability is present in the original stresses only (Figure 2(a)). Temporal phase is stable in winter and changeable in the warm months, both on synoptic and intraseasonal time scales (Figure 2(b)).

Contributions of the kth mode to stress vectors for the average temporal amplitude and zero temporal phase, $X_k(\mathbf{r}, t) = (A_k(\mathbf{r})e^{-i\varphi k})^* B_k e^{-i\phi k}$, B_k is average temporal amplitude $\phi_k = 0$, $k = 1, 2, 3,$ are computed. Due to

stability of the spatial phase, contribution of EOF 1 corresponds to the eastern wind for zero temporal phase (Figure 1(b)), shifting in time with its change (Figure 2(b)). The NW winds, with the temporal phase clustering around 135°, prevail in winter and winds, with the southern component and temporal phase between –135° and 0°, prevail in the warm season, when easterly winds, with temporal phase between 0° and 90°, also occur (Figure 2(b)).

EOF 2 features amplitude maxima over the northern land area and the southern JES, separated by a zonal minimum along 42°-44°N (Figure 1(b)). There is 180° phase shift between the cores, resulting in the oppositely directed stress vectors, related to this mode (Figure 1(b)). Temporal phase, accounting for the shifts of the entire pattern in time, varies strongly in the original fields, while in the filtered fields it tends to cluster around -180° (180°) in winter and around 45° in summer, with transition periods in spring and autumn (Figure 2(b)). Therefore, EOF 2 contributes eastern and western wind in the northern and southern cores, respectively, in winter, while in summer it is NW and southeastern (SE) wind, respectively (Figures 1 and 2).

EOF 3 occurs in the original data only and represents a synoptic divergence over the entire area (Figure 1). Both temporal amplitude and phase manifest strong variability but the phase tends to cluster around –45° in winter and between 45°and 135° in summer (Figure 2), corresponding to the convergence and divergence, i.e., anticyclonic (AC) and cyclonic vortex over the entire area in winter and summer, respectively.

Beyond the synoptic time scale, considerable contribution to the general wind direction over the JES could be imposed by the second mode only. On average, the temporal amplitude ratio B_1/B_2 is equal to ~2.5, while the spatial amplitude ratio A_1/A_2 is above 2, 1, and 0.6 northward of 41°-42°N, 38°-39°N, and 36°-37°N, respectively, i.e., wind shift due to EOF 2 is below 10°, 20°, and 35° in these areas. It is only in the southwestern (SW) area adjacent to the Korea Strait (south of 36°) that the wind shift can reach 40°. Thus, it may be concluded that prevailing wind directions can be analyzed from EOF 1 of low-pass filtered wind stresses alone.

4. Seasonal Wind Variation and Typical Patterns

To analyze seasonal wind variation, monthly histograms based on 5°-gradations of the PC 1 temporal phase from the filtered wind stresses are computed, with the phase transformed as $\phi' = -\phi + 90^{\circ}$, i.e., increasing clockwise from 0° through 360° and the zero phase corresponding to the northern wind (Figure 3). As expected, the NW mode is dominant from November through February, while the histograms are bi- or multimodal in other months; especially fuzzy structure occurs in April, June, and September. Western winds become frequent during the transition periods between the winter and summer monsoon, forming separate histogram modes in March and April, while merging into a single mode with NW winds in October. The SW mode is strongest from April through May, shifting towards southerlies in June, but other modes are non-negligible, for instance the east-northeastern and south-southeastern (SSE) modes in May (Figure 3). The SW and eastern modes are dominant in July. It is remarkable that the northeastern (NE) mode is strong in August, and September, while it was not so for the NCEP reanalysis winds [10]. The southern wind prevailing in monthly fields in summer [3, 8] is never a dominant mode and corresponds to the histogram minima in May, June, and September.

Patterns of seasonal wind shifts over the JES can be inferred from the PC 1 temporal phase (Figure 2(b)), in conjunction with the monthly histograms from the filtered stresses (Figure 3). From winter to spring, wind shifts counterclockwise from the northwest to southwest, further to the south/southeast by early summer, and to east/northeast by late summer. In fall, wind can shift further counterclockwise to the north and then northwest or it can shift clockwise from the southeast/east to southwest, west, and northwest. However, this pattern is interrupted by dramatic intra-seasonal wind shifts during summer monsoon, while switches between the counterclockwise and clockwise shifts occur in fall and reversals towards NW winds occur in spring, demonstrated by the nonmonotonic temporal phase (Figure 2(b)). Nevertheless, the first EOF mode can be considered as

the East Asia Monsoon pattern, with characteristic wind directions and seasonal shifts.

Statistical patterns of wind stress over the JES are derived by averaging of 6-hour filtered fields within histogram maxima. Averaging is performed within 35°-45° range of wind directions, which exceeds possible wind shift imposed by EOF 2 (Section 4). Wind stress curl, a principal factor affecting the oceanic circulation in general, is computed from the average wind stress. Typical wind stress and stress curl patterns (shown in Figure 4 for characteristic modes marked by circles in Figure 3) are, generally, similar to those earlier derived from NCEP reanalysis stresses, based on 5-8 clusters for every month, with equal direction ranges [10]. However, the pattern occurrences (shown in Figure 4) are justified by histogram modal structure (Figure 3).

Typical NW patterns, most frequent from October through March (Figure 3), are similar to monthly mean stresses from this data set (not shown) and from that of the European Center for Medium range Weather Forecasting (ECMWF) reanalysis [11]. In winter the cyclonic wind stress curl prevails, with local areas of AC curl (Figure 4 for January; see discussion of local features caused by adjacent land orography in Section 5), while in March, April, and September through November the AC curl prevails (Figure 4 for March and October). The western (zonal) pattern, frequent in the monsoon change periods, features the AC curl southward of 42°-43°N, while in the northern area the curl is mostly cyclonic, associated with the left-hand side of the wind jet shifting to the southwest there (Figure 4 for March).

The SW pattern features the dipole-shaped curl along the wind jet following the sea axis in April, May, and July (Figure 4 for July), while in June the histogram mode is shifted towards the southerlies (Figure 3) and the curl distribution of the SW pattern (Figure 4 for June) is similar to the W pattern. The SSE and eastern typical patterns, frequent in mid summer (Figure 3), manifest mostly cyclonic curl (Figure 4 for August and July,

respectively). The SSE pattern features a zone of the AC curl along the eastern coast, while the curl is anticyclonic northward of 45°N in the eastern pattern. Curl distribution in the NE pattern (Figure 4 for September), frequent in late summer (Figure 3), is opposite to that of the SW pattern.

5. EOF Patterns of Wind Stress Curl

The leading mode of wind stress curl (over the sea surface only) accounts for 16.5% of the total variance (Figure 5a; Table 1). The moderate variance fraction can be explained by high variability of wind stress curl even if the effect of weather systems is removed by low-pass filtering. The EOF 1 spatial pattern (Figure 5b) corresponds to the typical NW pattern for January (Figure 4) and to monthly patterns from the reanalyses (Section 4). PC 1 is strongly above zero during winter monsoon, on average from mid November through mid March, and is close to zero from April through October (its contribution to the curl field in different areas is shown in Figure 5(c)). This mode is strongest in the winters 2000/2001 and 2005/2006 but weak in the winters 2001/2002, 2006/2007, and 2007/2008. Note that in Vladivostok winter 2000/2001 was extremely cold [4].

The winter pattern features the prevailing cyclonic curl over the JES. (Note that, with the positive PC 1, positive and negative spatial values in Figure 5(b) correspond to the cyclonic and AC curl, respectively). There are several curl dipoles near the western coast. They are associated with NW wind jets blowing through orographic gaps near the high coast (land orography is overlain on EOF 1 in Figure 5(b)). The cyclonic (AC) curl is generated at the left-hand (right-hand) side of a wind jet, facing downstream. The strongest wind jet off the major gap northward from Vladivostok (marked in Figure 5(b)) is well known [3, 7]. Smaller jets and curl dipoles off narrow orographic gaps were not resolved by coarse reanalysis data [10]. An AC curl zone is stretched out along the western coast northward of 46°N.

There is a zone of the strong cyclonic curl stretched out off the East Korea Bay (EKB; marked in Figure 5(b)) across the JES towards the Honshu

coast. It is associated with convergence of the jets off the Vladivostok and North Korea gaps. A smaller scale zone of the cyclonic curl is stretched out off the Korea coast at 36°-37°N, the latitude of the East Korea Warm Current (EKWC) separation from the coast [1]. This feature is poorly reproduced in the NW typical pattern (Figure 4 for January), due to the contribution from the second stress mode in this area, as discussed in Section 3. However, this is the only discrepancy between two patterns.

EOF 2 and EOF 3 of wind stress curl are statistically significant and non-degenerate in the sense of errors (Table 1). However, the corresponding eigenvalues are closer to each other than to their neighbors (Figure 5(a)), motivating their joint consideration. The EOF 2 and EOF 3 spatial patterns feature large positive loadings southward and northward of 43°N, respectively, while EOF 3 is also strong in the western JES off the EKB (Figure 5(b)). To compare their impact on the curl field, contributions from the leading EOF modes in characteristic boxes are computed as $X_k^{(j)}(t) = (A_k(\mathbf{r}_j)B_k(t)$, where $A_k(\mathbf{r}_j)$ and $B_k(t)$ are the scalar EOF and PC, respectively, $k = 1, 2, 3$ is the mode number, $j = 1, 2, 3$ is the box number, and $\mathbf{r}_j$ stands for the box co-ordinates. These boxes (shown in Figure 5(b)) are located (1) in the central JES (40.25°N, 137.75°E), (2) northward of 43N° (45.75°N, 139.75°E), and (3) off the EKB (39.25°N, 130.25°E). The $X_1^{(j)}$ and $X_{2+3}^{(j)}$ (i.e., sum of $X_2^{(j)}$ and $X_3^{(j)}$) time series are shown in Figure 5(c), with $X_{2+3}^{(j)}$ put equal to zero when its absolute value is less than that of $X_1^{(j)}$.

Comparing correlations of $X_{2+3}^{(j)}$ with PC 2 and PC 3 (Table 2), it may be concluded that the second mode accounts for the curl over the central JES from late March through October when it is stronger than the winter mode, i.e., during the monsoon change and summer monsoon. It features the AC curl in October and late March and oscillates between the cyclonic and zero

curl in July through September (Figure 5(c)). The former is consistent with the prevailing AC curl in the typical NW and western patterns in late winter and fall, while the latter corresponds to the dominant cyclonic curl in the SSE and eastern patterns becoming frequent by late summer (Section 4; Figures 3, 4). In April this mode is weak, with the exception of 2000 and 2006 when it features the strong cyclonic curl (Figure 5(c)).

Northward of 43°N, the third mode, main contributor to the summer curl in this area (Table 2), manifests the same sign in the entire area, with the highest loadings in the western part (Figure 5(b)). It is characterized by strong intraseasonal variability, beyond the synoptic time scale, and features mostly cyclonic curl from late winter through early summer and AC curl in late summer. This is consistent with the western and SW patterns, frequent in spring and summer, as well as with the eastern and NE patterns, frequent from mid through late summer (Section 4; Figures 3, 4). An exception is the AC curl in late winter 2003, when the contribution from the summer mode exceeded that from the winter mode (Figure 5(c)). In the area off the EKB (box 3) an impact on the curl from EOF 2 and EOF 3 is of the same sign, with $X_{2+3}^{(3)}$ being positively correlated to both PC 2 and PC 3 (Table 2), while PC 2 and PC 3 themselves are orthogonal (correlation of –0.02) due to the EOF method requirement [9]. Therefore, in this area the curl follows temporal variation of both summer modes, being mostly cyclonic during summer monsoon. However, the curl is anticyclonic in late summer 2001, 2004, and 2006 when PC 2 was weak and PC 3 was strong (Figure 5(c)).

6. Conclusion

Multivariate analysis of wind stress and stress curl around the JES is performed using data of the 0.5°-gridded 6-hour QSCAT/NCEP Blended Ocean Winds from Colorado Research Associates, spanning the period from July 1999 through July 2009. Wind stress vectors are decomposed to EOF in the complex form, using spatial correlations within data, which facilitates detection of low-amplitude signals, such as weak winds. The leading mode, covering about 30% of the total variance for the original fields and above

50% if synoptic variability is removed by wavelet filtering, represents the East Asia Monsoon pattern with characteristic wind directions and seasonal shifts. The contribution from the higher modes is not significant. These results confirm the previous findings from NCEP reanalysis [10].

Typical patterns are computed by averaging 6-hour stresses within histogram maxima of wind directions, accounted for by the first complex EOF mode, with the synoptic variability filtered out. The typical patterns differ by general wind directions and curl distributions computed from average stresses. They are verified by the independent scalar EOF analysis of wind stress curl, over the sea surface only, derived from the same QSCAT/NCEP data set, with intra-monthly variability filtered out. The leading curl mode represents the winter pattern, with fine features resolved, such as several curl dipoles related to orographic gaps. The second and third modes together capture curl variability during the monsoon change and summer monsoon. Over most of the JES (southward of 43°N) they feature the prevailing AC curl in late winter and fall and mostly cyclonic curl in mid through later summer. Northward of 43°N the curl is mostly cyclonic from late winter through early summer and anticyclonic in late summer.

Wind stress curl is a major factor affecting the oceanic circulation in general. However, transport in the Korea Strait is usually considered as a forcing of the circulation in the southern JES, i.e., the Tsushima Warm Current (TWC) system, including the EKWC [1]. Still, an impact of wind stress curl upon the circulation is recognized, in the first place on the cyclonic gyres in the northern JES. Using oceanic models, it also was shown that in fall and winter the AC curl associated with the wind jet off Vladivostok was responsible for the AC sea circulation off North Korea [11, 10], such as formation of warm eddies and the NW branch of the subarctic front [2]. Numerical simulations also suggest a considerable effect of summer wind, in particular on the TWC path variation. It was shown that the EKWC weakened (intensified) under the forcing of the cyclonic (AC) wind stress curl [10]. This finding relies on typical patterns derived from the NCEP reanalysis which are now confirmed by the satellite winds.

References

[1] K.-I. Chang, W. J. Teague, S. J. Lyu, H. T. Perkins, D.-K. Lee, D. R. Watts, Y.-B. Kim, D. A. Mitchell, C. M. Lee and K. Kim, Circulation and currents in the southwestern East/Japan Sea: overview and review, Progress in Oceanography 61 (2004), 105-156.

[2] M. A. Danchenkov, V. B. Lobanov, S. C. Riser, K. Kim, M. Takematsu and J.-H. Yoon, A history of physical oceanographic research in the Japan/East Sea, Oceanography 19 (2006), 18-31.

[3] N. A. Dashko and S. M. Varlamov, Meteorology and climate, A. S. Vasilyev, F. S. Terziev and A. N. Kosarev, eds., Hydrometeorology and hydrochemistry of seas. Vol. 8. The Japan Sea. Iss. 1. Hydrometeorological conditions. Gidrometeoizdat, Sankt-Peterburg, Russia, 2003, pp. 19-103 (in Russian).

[4] C. E. Dorman, R. C. Beardsley, N. A. Dashko, C. A. Friehe, D. Kheilf, K. Cho, R. Limeburner and S. V. Varlamov, Winter marine atmospheric conditions over the Japan Sea, J. Geophys. Res. 109 (2004), C12011, doi:10.1029/2001JC001197.

[5] C. E. Dorman, R. C. Beardsley, R. Limeburner, S. M. Varlamov, M. Caruso and N. A. Dashko, Summer atmospheric conditions over the Japan/East Sea, Deep-Sea Research II. 52 (2005), 1393-1420.

[6] S. Yu. Glebova, Types of atmospheric processes over the seas of the Far East, interannual variability of their occurrence and contingency, Izvestiya TINRO 134 (2003), 209-257 (in Russian with English abstract).

[7] H. Kawamura and P. Wu, Formation mechanism of the Japan sea proper water in the flux center off Vladivostok, J. Geophys. Res. 99 (1998), 553-574.

[8] J.-Y. Na, J.-W. Seo and S.-K. Han. Monthly-mean sea surface winds over the adjacent seas of the Korea Peninsula, J. Oceanogr. Soc. Korea 27 (1992), 1-10.

[9] R. W. Preisendorfer, Principal Component Analyses in Meteorology and Oceanography, Elsevier, 1988.

[10] O. Trusenkova, A. Nikitin, and V. Lobanov, Circulation features in the Japan/East Sea related to statistically obtained wind patterns in the warm season, J. Mar. Sys. 78(2009), 214-225.

[11] J.-H. Yoon and Y.-J. Kim, Review on the seasonal variation of the surface circulation in the Japan/East Sea, J. Mar. Sys. 78 (2009), 226-236.

Table 1. Statistical significance of the leading modes derived from wind stress and stress curl: μ_k is the *k*th eigenvalue expressed as a fraction (%) of the total variance accounted for by the *k*th mode and $\Delta\mu_k = \mu_k(2/N^*)^{1/2}$ is its error [9], with $N^* = 180$ degrees of freedom. If $T_k = (\mu_k - \mu_{k+1})/(\Delta\mu_k + \Delta\mu_{k+1}) > 1$, an eigenvalue is non-degenerate $(\mu_k > \mu_{k+1})$. T^* is a threshold of statistical significance in terms of Monte Carlo testing: if $T^*_k > 1$ the *k*th eigenvalue is non-random [9]

Mode	$\mu \pm \Delta\mu$	T	T^*
	Original wind stresses		
1	26.5±3.8	3.4	29.1
2	12.5±1.3	1.8	9.2
3	8.5±0.9	2.0	5.1
	Low-frequency wind stresses		
1	50.2±5.3	4.9	35.1
2	16.0±1.7	4.7	11.6
	Low-frequency wind stress curls		
1	16.5±1.7	3.6	5.1
2	7.5±0.8	1.1	3.8
3	6.1±0.6	2.9	

Table 2. Correlation of $X_{2+3}{}^{(j)}$, $j = 1, 2, 3$ (boxes shown in Figure 5(b)), with PC 2 and PC 3. The 99% level of statistical significance for $N^* = 180$ degrees of freedom is equal to 0.22

	$X_{2+3}{}^{(1)}$, central JES	$X_{2+3}{}^{(2)}$, north of 43°N	$X_{2+3}{}^{(3)}$, east of EKB
PC 2	0.99	0.07	0.67
PC 3	–0.13	0.98	0.75

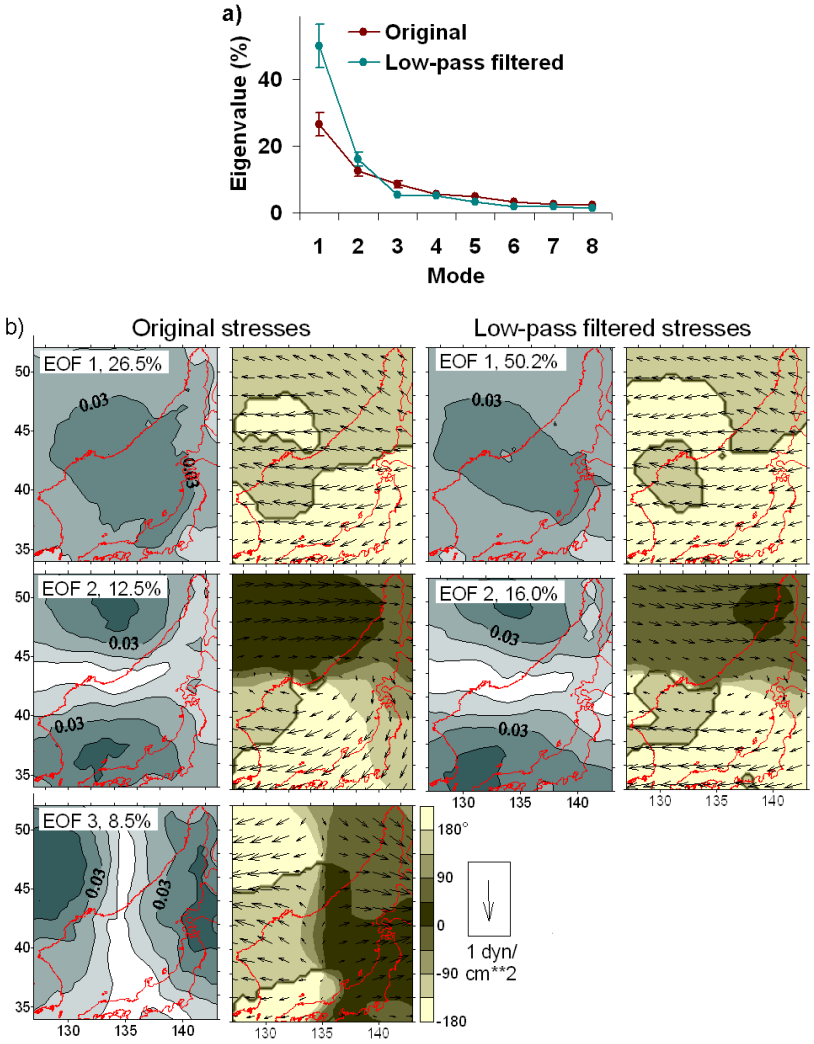

Figure 1. (a) Eigenspectrum (%) for the original (dark red) and low-pass filtered (blue green) wind stresses. (b) Spatial amplitudes (first and third columns; dimensionless; contours every 0.01, with the intensification to higher values) and phases (second and fourth columns; degrees) of the leading modes from the original and filtered stresses. Stress vectors (dyn/cm^2; every 9th vector shown) related to the corresponding mode for zero temporal phase and average temporal amplitude are overlain on the phase patterns. Reference vector corresponds to 1 dyn/cm^2.

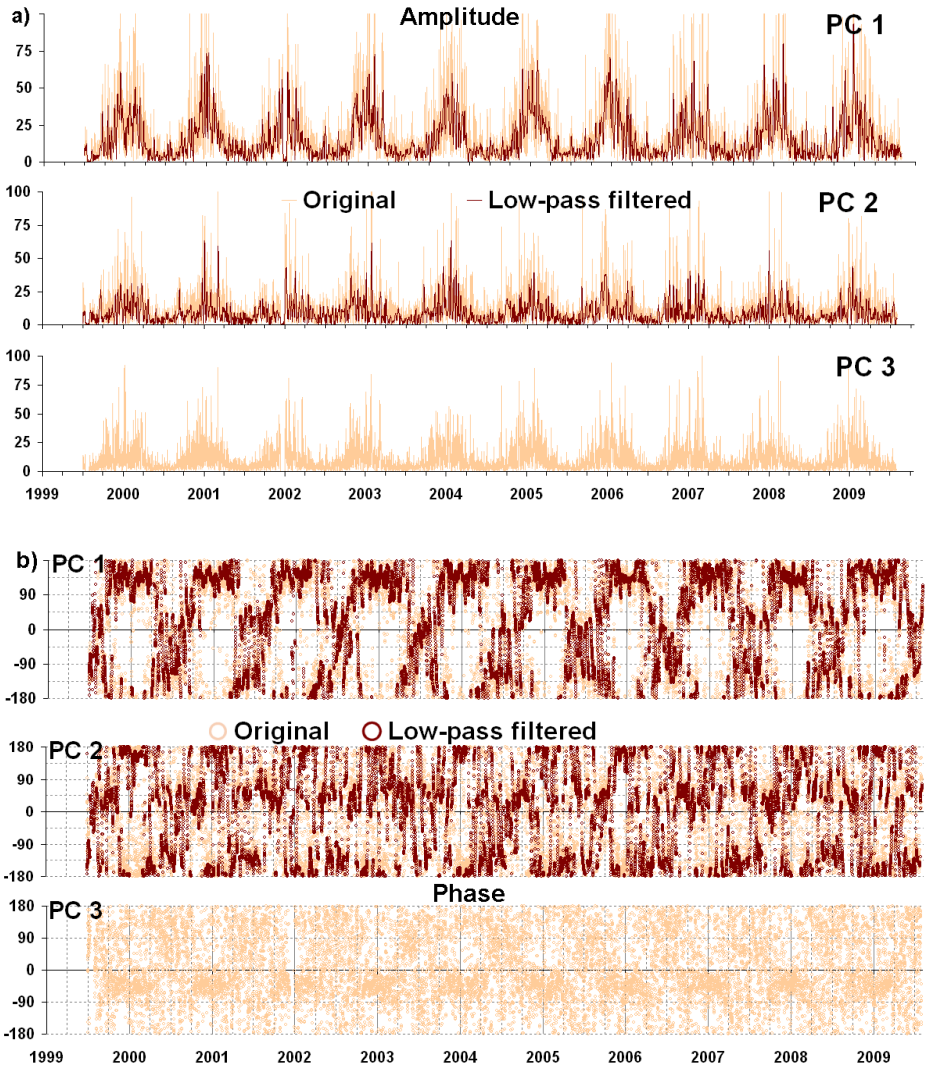

Figure 2. (a) Temporal amplitudes (dyn/cm^2) of the leading modes from the original (peach) and low-pass filtered (dark red) wind stresses. (b) Temporal phases (degrees) for the same modes for the original (peach circles) and low-pass filtered (dark red circles) stresses.

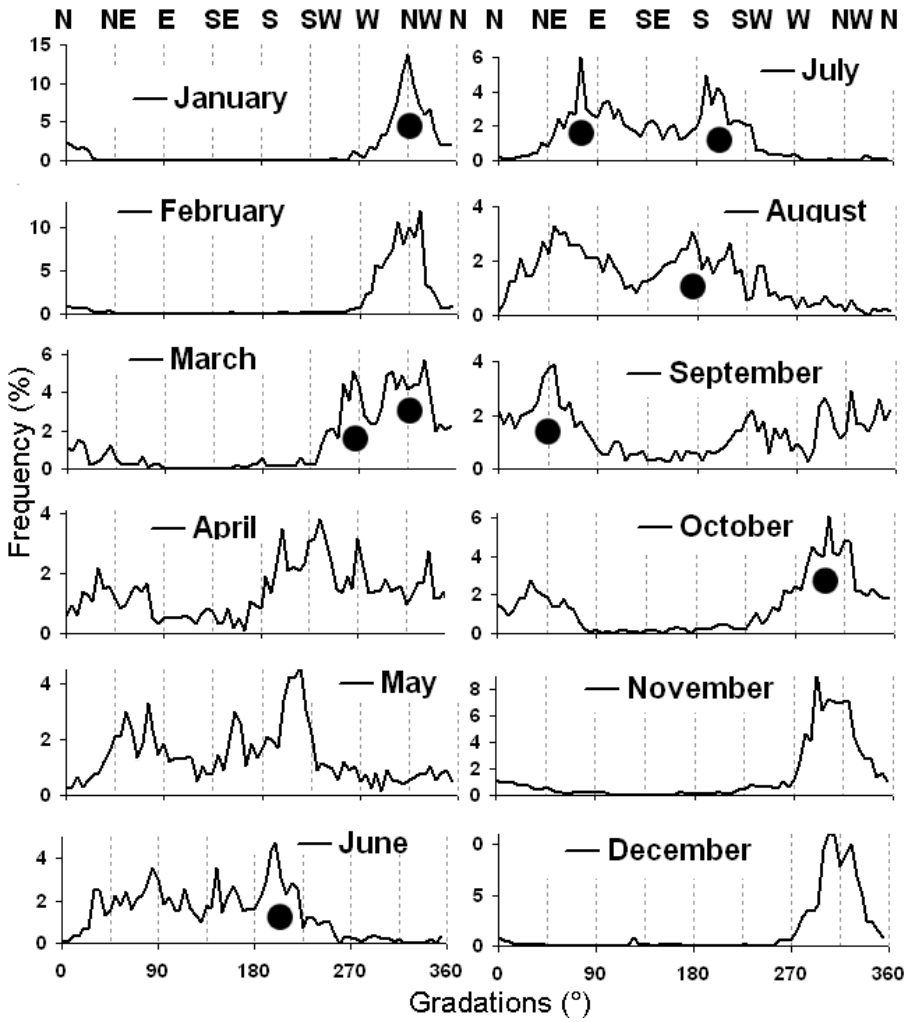

Figure 3. Monthly histograms based on 5°-gradations of the temporal phase of PC 1 from low-pass filtered wind stresses. The zero phase corresponds to the northern wind, increasing in the clockwise direction.

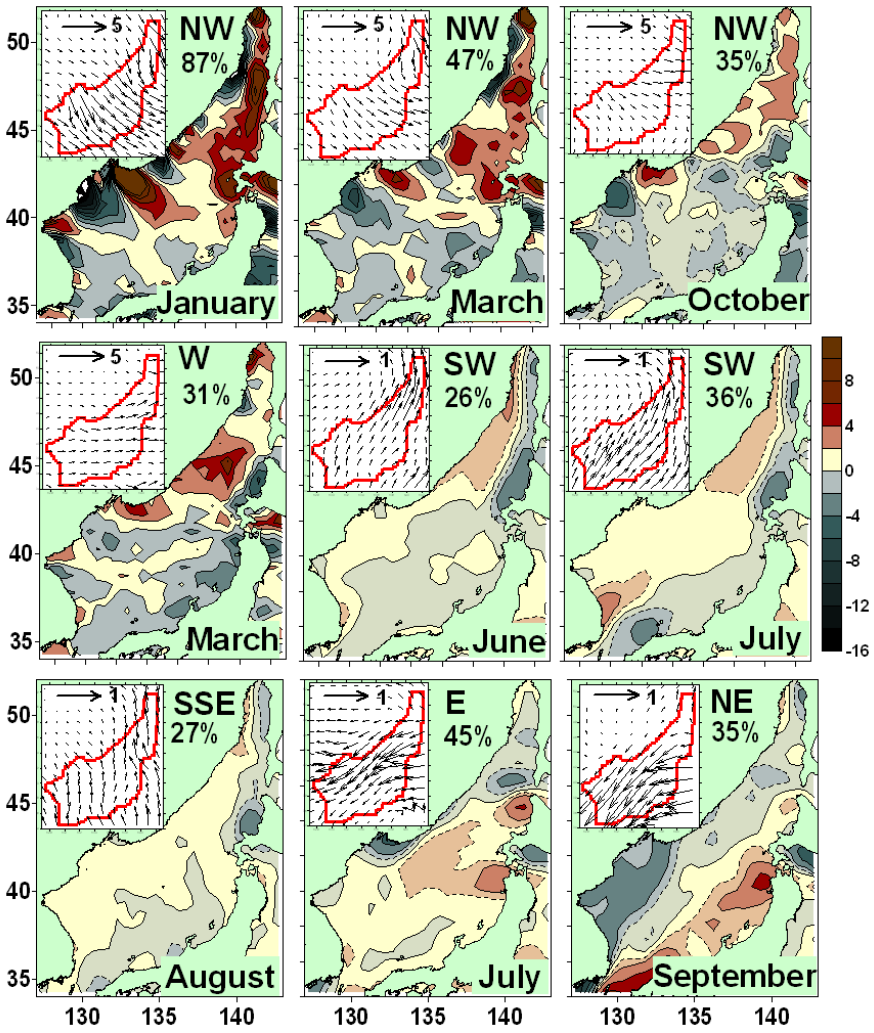

Figure 4. Typical patterns of wind stress (dyn/cm^2) and stress curl ($\times 10^{-8}$ dyn/cm^3) corresponding to the histogram modes marked by circles in Figure 3. Frequency of occurrence (%) is shown. Scale stress vectors correspond to 5 dyn/cm^2 for January, March, and October and to 1 dyn/cm^2 for other months. Cyclonic and AC curl is positive and negative, respectively. Curl contour interval is 2×10^{-8} dyn/cm^3; additional contours are dashed.

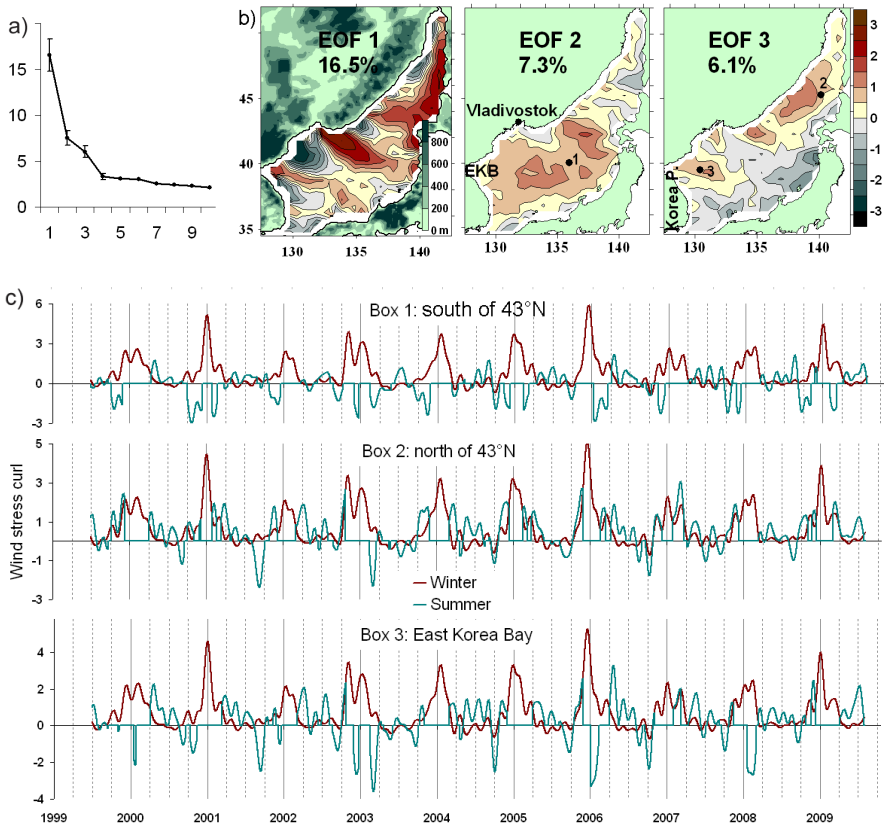

Figure 5. (a) Eigenspectrum (%) for wind stress curl. (b) spatial patterns ($\times 10^{-8}$ dyn/cm^3) multiplied by standard deviation of the corresponding PCs for modes 1 – 3 from curl. Land orography (m) is overlain on the EOF 1 pattern. Geographical features are marked. (c) Contributions ($\times 10^{-8}$ dyn/cm^3) of the winter (dark red) and summer (blue green) modes for boxes 1 – 3 (shown in Figure 5(b)). The summer mode contribution is equal to zero if its absolute value is below that of the winter mode. Cyclonic and anticyclonic curl is positive and negative, respectively.